BOLLETTINO DI GEOFISICA TEORICA ED APPLICATA VOL. XXXIII, N. 132 - DECEMBER 1991

L.I. PERLOVSKY

ACOUSTIC CRITICAL OPALESCENCE OF THE TRANSITIONAL UNDER-ICE LAYER IN THE ARCTIC

Abstract. Arguments are presented for the existence of an under-ice transitional layer, which significantly affects the under-ice acoustic wave propagation. We have developed a novel model based on the first principles of statistical physics that considers the transitional under-ice layer and the unconsolidated sea-bottom layer. This model predicts the existence of transitional layers, in which the transition from nonrigid, liquid phase to rigid phase occurs. It further predicts these transitions to be second order phase transitions, which leads to large scale spatial variations of rigidity. The statistical description of these variations is obtained and the parameters of the statistical description are related to the local environmental characteristics, such as the sea-bottom geology and the average turbulent energy in the under-ice environment. The predicted relations are in good agreement with the experimental data. We have calculated acoustic wave attenuation and phase variations due to scattering by rigidity variations and due to propagation in random transitional layers. Predictions of the developed theory are compared to the published experimental data. This comparison shows good agreement with the data on Arctic transmission loss and on random phase variations in the acoustic field.

INTRODUCTION

Under-ice acoustic wave propagation is characterized by an upward refracting environment, which causes a strong interaction of acoustic waves with the ice cover. This interaction scatters acoustic energy, which in turn causes energy transmission losses and creates spurious backscatter or reverberations (Urik, 1983). Characterization of these transmission losses, modeling ambient noise, and a stochastic description of reverberations present important problems in Arctic underwater acoustics. Major parts of these problems, which have not been fully resolved in past research are under-ice surface modeling and an accurate description of the interaction of acoustic waves with rough surfaces. The novel under-ice surface model suggested in this publication predicts statistical distributions of geometrical shapes and fluctuations (variations) of rigidity in the surface layer due to the rigid-nonrigid phase transition. The model also includes the relations between the model parameters and other environmental characteristics, such as the energy distribution on different scales. The scattering of acoustic waves by statistically-specified rough surfaces and by variations of rigidity in the surface layer is also calculated.

Another important characteristic of shallow water acoustic wave propagation is the bottom propagation of compressional and shear waves along refracted ray paths. These waves carry information about sources located in water in addition to information on the bottom environment. The scattering of these waves by bottom roughness and especially by rigidity variations (Perlovsky, 1986) adds to the specific reverberation characteristics of the shallow water environment.

Manuscript received October 27, 1991; accepted December 10, 1991.

Nichols Research Corporation, 251 Edgewater Drive, Wakefield, Massachusetts 01880, U.S.A..

Processes responsible for bottom roughness (Hamilton, 1980) are better understood than those responsible for ice roughness; however, modeling the variations of rigidity that occur in the bottom near the surface layer requires a novel approach, based on the theory of the second order phase transitions. This approach is developed in this publication for the shallow water Arctic environment.

Under-water acoustic propagation and interaction of acoustic waves with a rough ice boundary have been the subject of extensive research activity for over two decades. An overview of statistical approaches to the description of a rough ice surface can be found in Green (1984). Two types of statistical descriptions of rough surfaces are discussed in the literature. Discrete models characterize the under-ice surface by randomly distributed ice keels (Diachok, 1976; Wadhams, 1981; Hibler et al., 1972). Continuous statistical models describe the under-ice surface as a stochastic process and analyze it in terms of spatial autocorrelation functions or spatial spectra (Mellen, 1966; Hibler et al., 1972; Rothrock and Thorndike, 1980). In comparison with these previously suggested approaches, the unified approach that we have developed, in addition to its theoretical appeal, has the advantages of parsimonious use of parameters and the relation of model parameters to other local environmental characteristics, such as the environment energy, ocean currents, and winds. Our model considers a transitional nonrigid layer under ice and predicts the variations of rigidity due to second-order phase transitions between nonrigid and rigid phases. This will allow for the prediction of acoustic propagation losses, ambient noise and reverberation characteristics.

Under-ice acoustic propagation theory was recently advanced in the works by Kuperman and Schmidt (1986) and Schmidt et al. (1985). In this series of publications the full wave approach to acoustic propagation in stratified media with rough boundaries was developed. In these works the importance of the scattering of acoustic energy into shear waves was emphasized, in agreement with our results. Also, the Kirchoff approximation has been used in Kuperman and Schmidt (1986), which results in a simplification of the directional distributions of the scattered fields and, therefore, in deviations of the modeled reverberations from the true ones. An exact description of the interaction of acoustic waves with the under-ice surface was recently developed using a numerical finite difference model (Baggeroer and Fricky, 1988, private communication), which also proved the importance of the conversion of acoustic energy into shear waves. This model, however, cannot be extended beyond the scale of a few wavelengths because of the immense numerical complexity. This publication rigorously treats the scattering of acoustic waves by variations of rigidity. The scattering by rigidity variations, which is a unique feature of the developed approach, is expected to be responsible for directional properties of reverberations in the Arctic.

Propagation mechanisms and the frequency dependence of acoustic attenuation due to various mechanisms in the Arctic environment were considered recently by Duckworth and Baggeroer (1986). It was concluded that "much of the observed energy interacted with the upper 200 meters of sediments", which underlines the importance of modeling of rigidity variations in sediments that we developed. It was also concluded that available models do not provide an adequate parameterization of the frequency dependence of acoustic losses. We compared the predictions of our model to the experimentally derived data in Urick (1983) and Duckworth and Baggeroer (1986). Our model predicts that the scattering of acoustic energy into shear waves is the main attenuation mechanism, which explains the experimental evidence that there are relatively large transmission losses while the random phase variations of acoustic field in water column are relatively small. The comparison to experimentally derived data shows very good agreement.

In Section 2, the transitional layer under ice and the unconsolidated sedimentary layer of the sea bottom are considered. A novel theory of rigid-nonrigid transition in these layers is developed based on second order phase transition theory. This theory predicts large scale spatial variations of rigidity, which results in strong scattering of acoustic energy into shear waves. The scattering of acoustic waves by rigidity variations is considered in Section 3. Section 4 compares predictions of our theory to experimentally derived data. Our predictions are in a good agreement with the data.

RIGID-NONRIGID TRANSITIONS AND PROPERTIES OF TRANSITIONAL LAYERS

In this section the theory of rigid-nonrigid transitions is developed for the under-ice transitional layer and for the unconsolidated sediment layer on the sea bottom. We show that these transitions from nonrigid (fluid) phase to rigid compacted phase are second-order phase transitions, which results in large-scale spatial variations of the rigidity modulus. In Section 3 these variations will be shown to cause strong scattering of acoustic energy in the water column into shear wave energy in the ice and sea bottom.

This phenomenon has a classical textbook analogue termed "critical opalescence". An example of critical opalescence is provided by the water-steam transition. Consider a system of water and steam placed under pressure, always at the boiling point. As the pressure and temperature approach their critical values of 218 atm and 374°C, (Weast, 1981), the distinction between water and steam disappears, and the whole boiling phenomenon vanishes. At the critical point, the differences in density and volume energy between water and steam drop to zero, and bubbles of steam and drops of water intermix at all size scales from the macroscopic down to the atomic. In particular, drops and bubbles near micron size cause strong light scattering, called "critical opalescence", and the water and steam become nontransparent.

"Acoustic critical opalescence", or the reduction in transparency to acoustic waves at or near the critical point of the rigid-to-nonrigid phase transition, is discussed below.

The first and second order phase transitions

This subsection summarizes the terminology and phenomenology of phase transitions for the purpose of the current publication, a detail exposition can be found elsewhere, i.e. Landau and Lifshitz (1980a). The term "phase transition" is used to describe the discontinuous changes in physical properties of a substance that occur with the change of temperature without a change in chemical composition; a water-ice transition being an example. A state of a system when two phases can coexist in equilibrium is also called a phase transition. If the two phases are different in their energy and entropy per volume (which are the first derivatives of the Gibbs function), the phase transition is said to be of the first order. In such a transition the molecules on the surface between the two phases have an excess energy as compared to the molecules inside a continuous phase. This produces surface tension between the phases: the surface area tends to a minimum, therefore, phases tend to separate from each other and they do not intermix significantly. If the two phases have the same energy and entropy per volume but are different in the derivatives of these quantities (which are the second derivatives of the Gibbs function, i.e., thermal capacity), the phase transition is said to be of the second order. Second order phase transitions are characterized by the absence of surface tension between phases so that the phases can mix on all spatial scales. This happens at the critical point in a water-steam system where the phase transition is of the second order, and spatial variations of physical properties occur on all scales.

In the laboratory environment the ice-water phase transition is always of the first order. We will show below, however, that in the Arctic environment in the presence of turbulent energy this transition becomes a second order phase transition. The rigid-nonrigid transition in sediments is considered below first, because it is conceptually simpler.

Rigid-nonrigid phase transition in sediments

Consider the physical mechanisms responsible for rigidity in sediments. Little is known about the "rigidization" process in which shear coupling is formed between grains. Theories of adhesive and viscous friction mechanisms are well developed and are discussed by Lambe and Whitman (1969). However, as indicated in a review by Hamilton (1976), simple friction mechanisms are inadequate, and rigid bonds between grains are needed to explain the data on rigidity of marine sediments. The mechanisms that seem to be responsible for rigid bonds are cement deposition near grain contacts and grain deformation due to lithostatic pressure. If shear interactions between grains are mostly affected by pressure, the shear modulus primarily depends on the depth. If cementation is the main mechanism, the age of the rocks and other factors are more important. For any of these mechanisms, the process can be described by

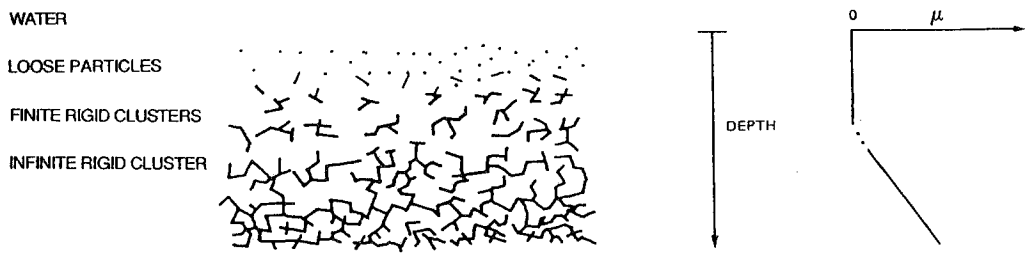

Fig. 1 — Rigid-nonrigid transition in sea-bottom sediments.

the probability of a bond between two neighboring grains.

Fig. 1 pictures sedimentary rock deposited as a single thick layer of loose sand or silt grains. The upper part, consisting of free grains, will not transmit shear waves: the shear modulus equals zero. Deeper, some adjacent grains bond into "clusters" of rigid phase, but the rigid phase is not yet continuous through the system, so macroscopically the shear modulus still is zero. Below a certain depth the rigid phase is continuous, and the shear modulus is nonzero. Being zero in one region and nonzero in the other, the shear modulus is not an analytic function. A singularity of this type causes a second-order phase transition, as was first shown by Landau in 1937 (Landau and Lifshitz, 1980a). The bond problem in percolation theory, which is quite similar to the problem of rigidity considered here, was first introduced by Broadbent and Hammersley (1956). They considered a geometrical stochastic process in which bonds are randomly formed between sites of a three-dimensional lattice. This problem was shown by Kasteleyn and Fortuin (1969) to be equivalent to other problems that are known to exhibit a second-order phase transition. In the rigidity problem we are considering, these results lead to the conclusion that near the transition point there are less-rigid "bubbles" and more-rigid "bubbles" in the rigid phase intermixed at all size scales, from the macroscopic down to the scale of the grains. These "bubbles" of near-acoustic wavelength size can cause strong scattering of acoustic waves, as sketched in Fig. 2.

Rigid-nonrigid phase transition in transitional under-ice layer

This section considers a phase transition in a relatively thin layer near the bottom of a multi-year ice, a layer that is near melting temperature. The ice-water phase transition in a laboratory environment is of the first order. Due to surface tension between ice and water the two phases do not mix. In the Arctic environment, however, turbulent flows in water under ice surface can mix the water and ice. Because the kinetic energy of an ice grain is proportional to its volume, and the surface tension between this grain and surrounding water or other ice grains is proportional to its surface area, it follows that surface tension dominates on small scales, while kinetic energy dominates on large scales. On small scales, therefore, rigid ice grains (crystals) are formed, while on large scales they are intermixed with water forming a transitional layer. The amount of water in this transitional layer might be small compared to the volume of ice. Because of the surface tension between differently oriented ice grains, thin liquid layers between ice grains exist at the melting temperature even in the absence of turbulent motion. The transitional layer exists only within the depth interval where the temperature is close to the sea-water freezing point, so that the ice and water phases are in equilibrium with each other.

The size of ice grains, r_{gr}, that are formed at the equilibrium (sea-water freezing) temperature is determined by the equilibrium between the grain surface tension energy

$$E_s \sim \gamma\, r_{gr}^2 \qquad (1)$$

and the average grain kinetic energy in the water environment

$$E_k \sim \epsilon\, r_{gr}^3 \,. \qquad (2)$$

The surface tension coefficient is $\gamma \simeq 30$ erg/cm^3 (Hobbs, 1974); amounts of air and salt

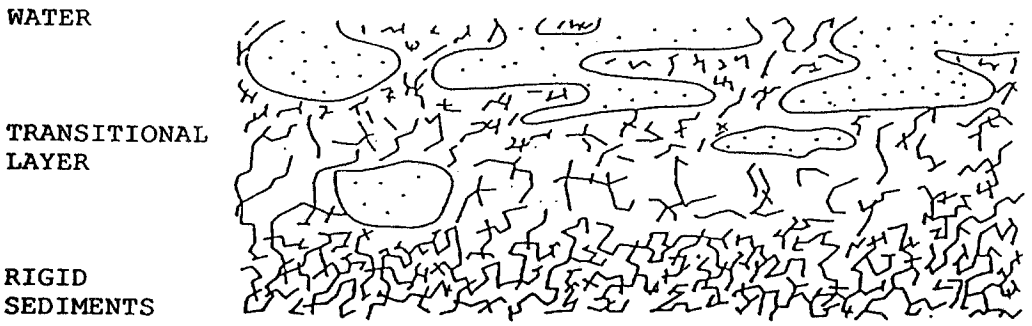

Fig. 2 — Unconsolidated sedimentary layer at the sea bottom in a state close to the rigid-nonrigid phase transition. Hence, there are long-scale variations in rigidity.

present in the ice might affect that value, however, no data were found to quantify these effects. The average kinetic energy per unit volume, ϵ, in the under-ice environment was reported in the literature to be within the range $\epsilon \simeq 7\text{-}70$ erg/cm^3, Hunkins (1980), depending on scale from centimeters to hundreds of meters; larger values of ϵ correspond to larger scales of turbulent flow. Equating (1) and (2) results in an estimate of the ice grain size:

$$r_{gr} \sim \gamma/\epsilon \ . \tag{3}$$

For the range of values of ϵ this estimate yields r_{gr} on the order of a few centimeters or smaller. The energy density ϵ must be taken over a volume on the order of a grain size, so it is necessary to use the smallest value $\epsilon \simeq 7$ erg/cm^3, corresponding to the smallest scale. This results in an order of magnitude estimate of $r_{gr} \sim 4$ cm. A more accurate estimate of grain size accounting for the degrees of freedom in the system (Floyd, private communication, 1988) can be obtained as follows. Formation of a rigid bond between two ice grains eliminates ΔDOF degrees of freedom. Assuming equipartition of energy between these degrees of freedom results in the following change in the Gibbs function

$$\Delta G_{DOF} = \Delta DOF * \epsilon * V \ , \tag{4}$$

where $\epsilon = 7$ erg/cm^3 as discussed above and V is the grain volume. Ice grains in a columnar or dendritic zone (Gow et al., 1980) are of an elongated shape since ice grows preferentially in a vertical direction, perpendicular to the C-axis; there are indications that the C-axis of ice crystals tend to be oriented along the direction of flow; however, we will not account for these complications here because there is no sufficient data to verify the effects of this anisotropy on acoustic wave propagation. Also, we will not account for complicated shapes of ice grains shown in Figs. 3a, and 3b. The following calculations are performed for hexagonal prism ice grains, Fig. 3c; similar calculations repeated for spherical, cubic, and square prism ice grains all yield very similar results. This further justifies a simplifying isotropic assumption which seems reasonable for the purpose of this publication. The volume of hexagonal prism grains in Fig. 3c is given by:

$$V = 3\sqrt{3}/2 \ (r_{gr}/2)^2 \cdot \ell \ . \tag{5}$$

For elongated grains, formation of a rigid bond affects only horizontal degrees of freedom, ΔDOF ~ 2 to 4. In addition to the DOF change, the formation of a rigid bond between two grains results in a decrease of the surface energy with a corresponding change in the Gibbs function

$$\Delta G_E = -2\gamma A \ , \tag{6}$$

where A is the single grain surface area change. According to Fig. 3c:

$$A = r_{gr} \cdot \ell/2 \ . \tag{7}$$

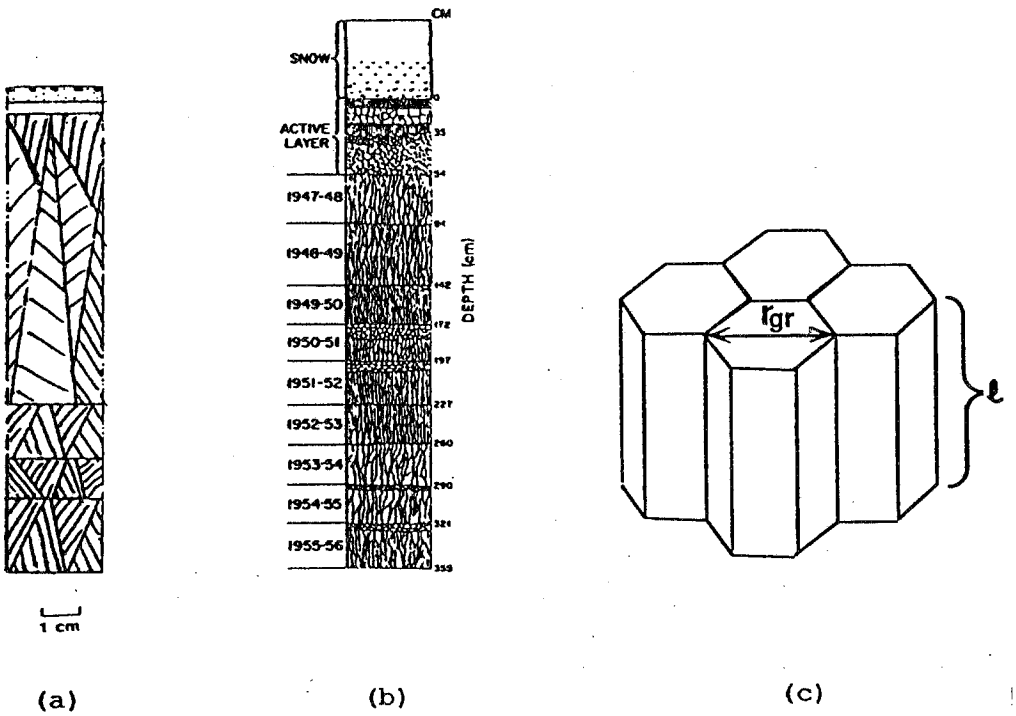

Fig. 3 — Examples of multiyear ice structures; (a) from Gow et al. (1987) and (b) from Cherepanov (1957); a simplified picture of ice grain (c) provides for an approximate estimation of the grain size r_{gr}, as explained in the text.

Combining eqns. (4) through (7), the total change in the Gibbs function due to the formation of a rigid bond is

$$\Delta G=\Delta G_{DOF}+\Delta G_E=\Delta DOF_*\epsilon_*\ (3\ \sqrt{3}/2\ (r_{gr}/2)^2\ )\ell-\gamma r_{gr}\cdot\ell. \tag{8}$$

The equilibrium size of ice grains corresponds to $\Delta G=0$, which results in

$$r_{gr}=0.4\ \Delta DOF\ \gamma/\epsilon=1.6\ to\ 3.2\ cm. \tag{9}$$

As mentioned above, this result is not sensitive to particular ice grain shapes. For various shapes, including spheres, cubes, and square prisms, the estimated value of r_{gr} is between 1.5 and 4 cm. On scales larger than r_{gr} the kinetic energy dominates, the process is of the second order, and ice and water mix in the transitional layer, resulting in spatial variations of rigidity similar to those in Fig. 2.

The dissolution of salt, which is initially entrapped within the ice during freezing, enhances the process of mixing of ice and water and might increase the thickness of the transitional layer. Most of the salt in the ice is contained in brine pockets separated by ice plates; this substructure of ice grains is important for scattering of high frequency acoustic waves ($\sim$100 kHz) by the ice surface (Stanton et al., 1986). This effect does not significantly affect relatively low frequencies ($\sim$10Hz) that dominate the long-range acoustic propagation in the Arctic, which is considered in this paper.

The theory developed in this section does not account for the diversity of conditions determining real process of congelation ice growth. Above, the arguments are presented for the second order phase transition taking place near the bottom of the sea ice, and an approximate length scale at which the phase transition nature changes is estimated. This theory is supported

by the evidence that the mean ice grain diameter near the bottom of the thick ice cover is about 2 cm (Weeks, 1986), and that at temperatures close to the melting temperature all polycrystalline ice has liquid layers at the grain boundaries (Weeks and Mellor, 1983).

Second-order phase transitions

A theory of second-order phase transitions has been developed during this century by a number of researchers. Wilson (1983) provides an account of their work. A summary follows of those aspects of the theory that are essential for the purpose of this publication.

The rigidity problem, as formulated above, is a percolation theory problem, which can be characterized by the probability, p, of a rigid bond between two grains. There is a critical value of that probability, p_c, such that for $p < p_c$ only finite-size rigid "clusters" of connected grains exist, and the macroscopic shear modulus equals zero. For $p > p_c$, there is a nonzero fraction of grains that belong to an infinite rigid cluster; that fraction is denoted P (p), because it is a function of the bond probability p. The value P (p) determines the rigidity of a rock on a macroscopic scale. As had been discussed by Perlovsky (1986), the results of Kasteleyn and Fortuin (1969) are applicable in our case, and consequently, it can be concluded that the shear modulus, μ, is proportional to P (p). The coefficient of proportionality, denoted by μ_{gr}, corresponds to crystal ice, or for the case of sea bottom can be found from consolidated rock samples with zero or very low porosity, in which case P (p) ~ 1:

$$\mu = \mu_{gr} \cdot P\ (p). \tag{10}$$

For the case of the sea bottom the rigidity of a cement is usually lower than that of the grains, so μ_{gr} should be somewhat smaller that the grain shear modulus.

It has been established by Wilson (1983) that the functional dependence of P on p is given by

$$\begin{aligned} &P = (p - p_c)^{\beta}, \quad p > p_c; \\ &P = 0, \qquad\quad p < p_c. \end{aligned} \tag{11}$$

While eqns. (10) and (11) yield an average value of the shear modulus, μ, the variations or deviations, $\delta\mu$, of the shear modulus from its average value are also important as p approaches its critical value, p_c. These variations can be characterized by a correlation function between the variations of the shear modulus at two points, $\mathbf{r}_1$ and $\mathbf{r}_2$:

$$<\delta\mu\ (\mathbf{r}_1) \cdot \delta\mu\ (\mathbf{r}_2)> = \mu_{gr}^2\ G\ (r),\ r = |\mathbf{r}_1 - \mathbf{r}_2|. \tag{12}$$

Brackets $<\ldots>$ denote a statistical average. The shear modulus correlation is expressed in terms of a geometric correlation function, G (r), between bonds:

$$G\ (r) = \left(\frac{r_{gr}}{r} \right)^{1+\eta} \cdot exp\ (-r/r_c),\quad r_c = r_{gr} |p - p_c|^{-\nu}, \tag{13}$$

where r_{gr} is the grain size, and r_c is the correlation length.

The quantities, ν, β, and η, in eqns. (11) and (13) are called "critical exponents". Their values have been calculated by a number of authors; we use the value of η calculated by Colot et al. (1975) utilizing a modification of Wilson's ϵ-expansion scaling procedure, and the results of Monte-Carlo calculations by Levinshtein et al. (1975) for the values of ν and β:

$$\beta = 0.35 \pm 0.05,\ \nu = 0.80 \pm 0.05,\ \eta = 0.047 \pm 0.006. \tag{14}$$

The relation of this fluctuation theory to the present case can further be clarified if the applicability limits of the theory are considered. Eqns. (11), (13), and (14) above are valid near the transition

point when

$$|p-p_c| << 1. \tag{15}$$

Specifying this valaue to be less than, say, 0.1, and using eqns. (10) and (11) and the value of β above, we have

$$\mu/\mu_{gr} \leq 0.45 . \tag{16}$$

The shear-wave velocity in the transition layer, C_s , and the shear-wave velocity in rigid grains, C_{gr} , are given by

$$C_s^2=\mu/\varrho \quad , \quad and \; C_{gr}^2=\mu_{gr}/\varrho , \tag{17}$$

where ϱ is the density. The restriction follows that

$$C_s<0.7\ C_{gr} . \tag{18}$$

Inequality (18) holds true for unconsolidated sediments and as we are going to show immediately is also true for the under-ice transitional layer, so the theory is applicable for the considered conditions.

Eqns. (10) through (14) can be used to derive the relation between the shear wave velocity in the transitional layer C_s and the correlation length r_c :

$$C_s=C_{gr}\ (r_{gr}/r_c)^{\beta/2\nu} . \tag{19}$$

Taking the calculated value for $r_{gr}=2$ cm, eqn. (9), the average value for the shear wave velocity in an ice crystal $C_{gr}=2.0$ km/s, (Weeks and Mellor, 1983), and the correlation length of $r_c=20$ m, estimated from the Arctic data (Mellen and Di Napoli, 1984), eqn. (19) results in an estimate of the shear wave velocity in the under-ice transient layer:

$$C_s^i \approx 0.46\ km/s. \tag{20}$$

This satisfies the inequality (18).

In the case of the sea-bottom the shear wave velocity was measured for a variety of conditions and therefore eqn. (18) can be used to estimate the correlation length. Taking the values of $C_s^b=0.2$ km/s, and $r_{gr}=0.05$ mm, which are characteristic of the upper 35 m silty sediment layer in the Arctic Abyssal Plain (Vogt, 1986), a correlation length of 1.5 m for the spatial velocity variations in the sea bottom is obtained:

$$r_c=r_{gr}\ (C_{gr}/C_s)^{2\nu/\beta} \approx 1.5\ m . \tag{21}$$

These relations are used in Section 4 to relate acoustic propagation properties to the environmental characteristics.

MODEL FOR ACOUSTIC PROPAGATION WITH TRANSITION-LAYER BOUNDARIES

In this section a rigorous model is developed for acoustic propagation with rough boundaries specified as transitional layers according to the theory developed in the previous section. Two effects are calculated: acoustic plane wave attenuation and acoustic plane wave phase fluctuations due to propagation and scattering in transitional layers. It is shown that the main effect of acoustic propagation in a transitional layer is attenuation due to scattering into shear wave energy. Therefore, accurate calculation of these effects is possible using Born and eikonal approximations. These two effects were selected for calculation for the two following reasons. First, these effects

can be isolated in experimental data, therefore it is possible to verify predictions of our theory; this will be done in Section 4. Second, these calculations are important steps toward the development of the field theoretical model (Perlovsky, 1988), also the calculated reflection coefficient can be incorporated into normal mode solution via relection-coefficient boundary conditions (Koch et al., 1983).

Attenuation due to scattering by variations of the shear modulus

The wave equation in elastic isotropic media can be written as follows (Aki and Richards, 1980; Landau and Lifshitz, 1980c):

$$\varrho\ \ddot{u}_i = \partial_k\ \sigma_{ik}\ , \tag{22}$$

$$\sigma_{ik} = K\ e_{nn}\ \delta_{ik} + 2\ (\mu+\delta\mu)\ (e_{ik} - \frac{\delta_{ik}}{3} e_{nn})\ , \tag{23}$$

$$e_{ik} = \frac{1}{2}(\partial_i\ u_k + \partial_k\ u_i)\ . \tag{24}$$

Here and below ϱ is density; u_i is a vector of particle motion in the wave; σ_{ik} is the stress tensor; e_{ik} is the strain tensor; and ∂_k denotes derivatives with respect to the coordinates. All subindexes take values 1, 2, 3, or x, y, z and summation over repeated indexes is assumed. The bulk modulus K is considered constant, and the shear modulus $\mu+\delta\mu$ is divided into a constant part μ and a varying part $\delta\mu$, chosen so that the average $<\delta\mu>=0$, in accordance with eqn. (12).

In order to obtain the solution for the scattered fields, following Morse and Feshbach (1953), we write the particle motion vector as a sum of the incoming acoustic wave and two outgoing acoustic and shear waves:

$$u = u^{in} + u^{out,\ \ell} + u^{out,\ s}. \tag{25}$$

Then we substitute eqns. (23), (24), and (25) into eqn. (22) keeping in mind that $\ddot{\mathbf{u}} = -\omega^2\mathbf{u}$, $\partial_k\ u_i^{in} = ik_k\ u_i^{in}$, and for the acoustic incident field $\mathbf{k}\cdot\mathbf{u}^{in} = ku^{in}$, and $\mathbf{k}\ (\mathbf{k}\cdot\mathbf{u}^{in}) = -\Delta\mathbf{u}^{in}$ where Δ is the Laplace operator. This results in the following equation:

$$-\omega^2\ \varrho\ (u_i^{in} + u_i^{out}) = [K + \frac{4}{3}\ (\mu+\delta\mu)]\ (\Delta u_i^{in} + \Delta u_i^{out,\ \ell})$$

$$+\ (\mu+\delta\mu)\ \Delta u_i^{out,\ s} + (2i\ \partial_k\ \delta\mu)\ [k_i\ u_k^{in} - \frac{1}{3}\ \delta_{ik}\ k\ u^{in}]. \tag{26}$$

It is shown below that the scattered fields are much smaller than the incident acoustic field, therefore terms $\sim\delta\mu u^{out}$ can be neglected. The incident acoustic field satisfies the unperturbed wave equation with $\delta\mu=0$, therefore all terms $\sim Ku^{in}$, and $\sim\mu u^{in}$ cancel out. The resulting equation can be separated into two equations for acoustic and shear scattered fields as in Morse and Feshbach (1953):

$$(\Delta + k^2)\ u_i^{out,\ \ell} = \frac{k'_i\ k'_k}{k^2\ (K + \frac{4}{3}\ \mu)}\ [\frac{4}{3}\delta\mu\ k^2\ u_k^{in}$$

$$-(2i\partial_n\delta\mu)\ (k_k\ u_n^{in} - \frac{1}{3}\ \delta_{kn}\ ku^{in})], \tag{27}$$

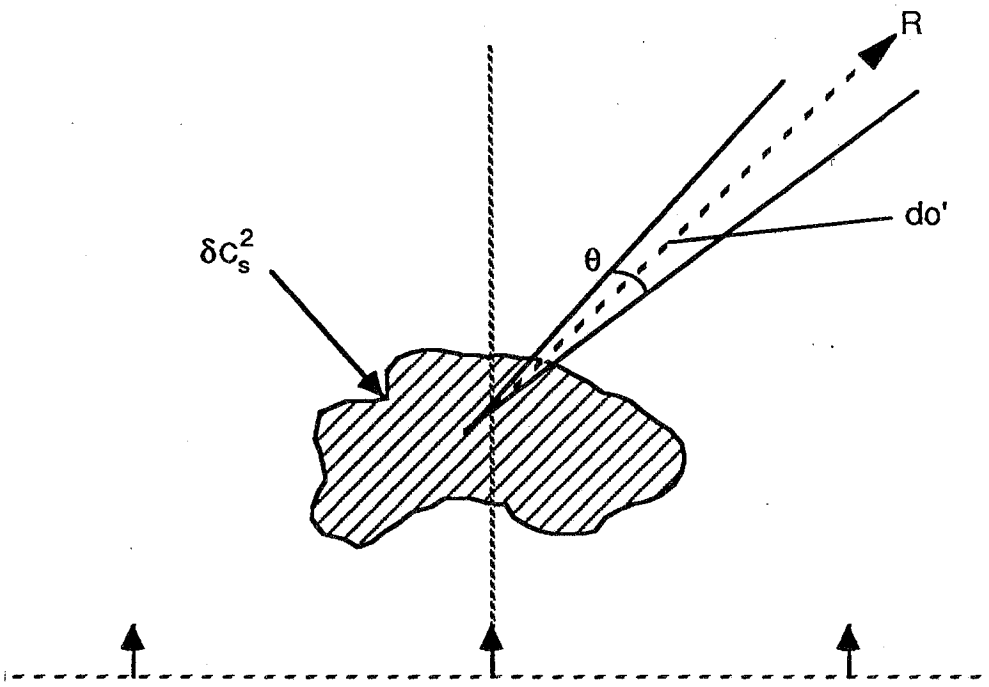

Fig. 4 — Upgoing incident wave scattered by a variation of the shear modulus, $\delta\mu$; the corresponding variation in shear-wave velocity is δC_s^2.

and

$$(\Delta+k'^2)\, u_i^{out,\,s}=(\delta_{ik}-\frac{k'_i\,k'_k}{k'^2})\,\frac{1}{\mu}\,[\,\frac{4}{3}\quad\delta\mu\;k^2\;u_k^{in}$$

$$-(2i\;\partial_n\;\delta\mu)\;(k_k\;u_n^{in}-\frac{1}{3}\delta_{kn}\;k\;u_{in})]\;. \tag{28}$$

In these equations **k'** are wave-vectors of the outgoing waves, $k'^2=k^2=\omega^2\varrho/(K+\frac{4}{3}\mu)$ for the scattered acoustic wave, and $k'^2=\omega^2\varrho/\mu$ for the scattered shear wave. The projection operators $(k'_i k'_k/k^2)$ and $(\delta_{ik}-k'_i k'_k/k'^2)$ assure the proper separation of the two fields.

The velocities of the two waves are

$$C_\ell^2=(K+\frac{4}{3}\mu)/\varrho,\;C_s^2=\mu/\varrho. \tag{29}$$

For simplicity let us consider first the solution of eqn. (27) at near-forward angles. Then terms $\sim\partial\delta\mu$ are neglected and the equation is written as

$$(\Delta+k^2)\;u^{out,\,\ell}=\frac{4}{3}\frac{\delta\mu}{\varrho C_\ell^2}\,k^2u^{in}. \tag{30}$$

The solution of this equation is well known; it can be obtained with the scalar Helmholtz equation Green function (Hobbs, 1974). Denoting the amplitude of the incoming wave by u_o^{in}, the field scattered by the rigidity variation at a distance R into a spherical angle do', as in Fig. 4, can be described as

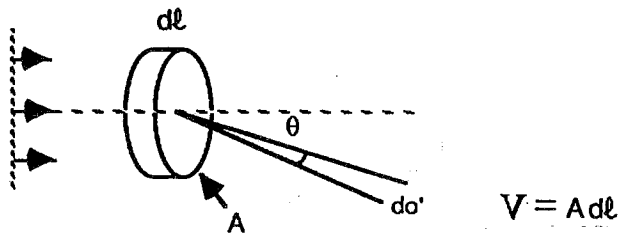

Fig. 5 — Scattering volume and angles.

$$u^{out,\ell} = -\frac{e^{ik'R}}{4\pi R}\ \frac{4}{3}\ \frac{k^2}{\varrho C_\ell^2} u_o^{in} \int_V \delta\mu\ (\boldsymbol{r})\ e^{i(\boldsymbol{qr})}\ d^3\boldsymbol{r},\ \boldsymbol{q}=\boldsymbol{k}-\boldsymbol{k}'. \tag{31}$$

Here the integration is over the rigidity variations volume, V, and the integral is the Fourier transform of the rigidity variations:

$$\delta\mu_{\boldsymbol{q}} = \frac{1}{\sqrt{V}} \int_V d^3\boldsymbol{r}\ e^{i(\boldsymbol{qr})}\ \delta\mu(\boldsymbol{r}). \tag{32}$$

As one would expect, the average value of the scattered amplitude $u^{out,\ell}$ is zero. This follows from eqn. (31), because the average rigidity modulus variation equals zero, $<\delta\mu>=0$. A useful average quantity is the energy extinction coefficient, di, which is the ratio of the average flux of energy scattered by a layer of media of thickness dl and area A into the angle do' to the incident energy flux, Fig. 5:

$$di = \frac{<dJ^{out}>}{J^{in}}\ . \tag{33}$$

These energy fluxes are given by, (Landau and Liftshitz, 1980b):

$$J^{in} = |\boldsymbol{u}^{in}|^2 \varrho\ \omega^2 C_\ell A,\ dJ^{out} = |\boldsymbol{u}^{out}|^2\ \varrho\omega^2\ C^{out}\ R^2\ do', \tag{34}$$

where C is the wave velocity in the media.

Substituting eqn. (34) into eqn. (35) results in

$$di = \frac{<|\boldsymbol{u}^{out}|^2>\ R^2\ do'\ C^{out}}{|\boldsymbol{u}^{in}|^2\ A\ C_\ell}\ , \tag{35}$$

This can be calculated from eqn. (31) for the outgoing acoustic wave, $C^{out} = C_\ell$, at near forward angles:

$$di_o = \frac{16}{9}\ \frac{k^4}{(4\pi)^2\ \varrho^2\ C_\ell^4} <|\delta\mu_{\boldsymbol{q}}|^2>\ do'\ dl. \tag{36}$$

A similar expression for the Rayleigh scattering of light was first derived by Einstein (1910).

In order to anticipate the modifications to this formula for nonforward angles and for scattering

into shear waves it is useful here to review various terms in this expression: the terms $(4\pi\varrho)^{-2}$ do' dl are due to the scattering kinematick, k^4 is due to $k^2 u^{in}$ in the wave eqn. (37), and $<|\delta\mu_q|^2>$ describes the rigidity variations, these terms will not be modified; $16/9C_\ell^4$ is due to scattering into acoustic waves, scattering into shear waves is proportional to $1/C_s^4$ instead and is orders of magnitude stronger than scattering into acoustic waves because $C_s/C_\ell << 1$. An additional factor fo C_ℓ/C_s appears below in eqn. (46) for shear waves due to energy fluxes. Before introducing these modifications, let us first calculate $<|\delta\mu_{\mathbf{q}}|^2>$, the spatial spectrum of rigidity variations, using eqns. (32) and (12):

$$<|\delta\mu_q|^2> = \frac{1}{V}\int_V d^3\mathbf{x} \int_V d^3\mathbf{x}' \; <\delta\mu(\mathbf{x})\,\delta\mu(\mathbf{x}')> \; e^{i(q(x-x'))} \tag{37}$$

$$= \frac{1}{V}\int_V d^3\mathbf{x} \int_V d^3\mathbf{x}' \; \mu_{gr}^2 \, G(|\mathbf{x}-\mathbf{x}'|) \; e^{i(q(x-x'))}.$$

The integrand here depends only on the difference $\mathbf{x}-\mathbf{x}'$; changing to new variables $\mathbf{r}=\mathbf{x}-\mathbf{x}'$, using eqn. (13), and spherical coordinates, this can be written as:

$$<|\delta\mu_q|^2> = \mu_{gr}^2 \, r^{1+\eta}_{gr} \int_o^{2\pi} d\varphi \int_o^{\pi} d\cos\theta \int_{r_{gr}}^{\infty} r^2 \, dr \; r^{-1-\eta} \; exp(-r/r_c + iqr\cos\theta) \tag{38}$$

$$= \frac{2\pi\mu_{gr}^2 \, r_{gr}^{1+\eta}}{iq} \int_{r_{gr}}^{\infty} dr \; r^{-\eta} \; e^{-r/r_c} \; (e^{-iqr} - e^{iqr}).$$

Since η is very small, eqn. (14), this integral can be evaluated analytically, by approximating a very slow varying term $r^{-\eta}$ with a constant $r_c^{-\eta}$, because the major contribution to this integral is due to the region $r \sim r_c$. (Numerical values used in the next Section 4 are obtained by numerical integration and are very similar to the analytical results obtained here.) The final expression for the rigidity variation spectrum is

$$<|\delta\mu_q|^2> = 4\pi\mu_{gr}^2 \left(\frac{r_{gr}}{r_c}\right)^{\eta} r_{gr} \, r_c^2 \frac{1}{1+q^2 r_c^2} \, . \tag{39}$$

Substituting this expression into eqn. (36) we obtain for the scattering into acoustic waves at near forward angles:

$$di_o = \frac{16}{9} \frac{k^4}{4\pi} \left(\frac{C_{gr}}{C_\ell}\right)^4 \left(\frac{r_{gr}}{r_c}\right)^{\eta} r_{gr} \, r_c^2 \frac{do' \, d\ell}{1+q^2 r_c^2} \, . \tag{40}$$

A similar formula for critical opalescence of electromagnetic waves was first derived by Ornstein and Zernike (1980), in the approximation $\eta = 0$.

Let us now account for the necessary correction at nonforward angles. Terms $\partial\delta\mu$ in eqn. (27) can be accounted for by evaluating the integral in eqn. (31) by parts. This will result in

$$-i\partial_n \, \delta\mu \rightarrow q_n \, \delta\mu. \tag{41}$$

Taking the definition of $\mathbf{q}=\mathbf{k}'-\mathbf{k}$ in eqn. (31) and expressing all dot-products in terms of

the scattering angle θ between the vectors **k** and **k'** (Fig. 5), the following expression for the scattering into acoustic waves at all angles is derived:

$$di_\ell = \frac{k^4}{\pi}\left(\frac{C_{gr}}{C_\ell}\right)^4 \left(\frac{r_{gr}}{r_c}\right)^\eta r_{gr}\, r_c^2 \frac{[(\cos\theta)^2 - 1/3]^2\, d\varphi\, d\cos\theta\, d\ell}{1 + 2k^2\, r_c^2(1-\cos\theta)} \quad . \tag{42}$$

We substitute here $k = 2\pi f/C_\ell$, where f is the frequency of the incoming wave, and we integrate over $d\varphi$ since there is no azimuthal dependence in this formula. These results in the final expression for the fraction of acoustic energy scattered into acoustic waves at an angle θ

$$di_\ell = 32\pi^4 \frac{r_{gr}\, r_c^2}{C_\ell^4}\left(\frac{C_{gr}}{C_\ell}\right)^4 \left(\frac{r_{gr}}{r_c}\right)^\eta \frac{[(\cos\theta)^2) - 1/3]^2\, d\cos\theta\, d\ell}{1 + 2(2\pi r_c/C_\ell)^2 f^2 (1-\cos\theta)} \quad . \tag{43}$$

If integrated along the ray path $d\ell$ in the transitional layer this expression specifies the angular distribution of Arctic reverberations due to scattering into acoustic waves in the previously discussed approximation. Other contributions to the reverberations, modifications of this result for normal modes, and the methodology to account for rough boundaries in a more rigorous way are discussed in Perlovsky (1988). The numerical value of eqn. (43) is much smaller than 1 (see Section 4), therefore, the Born approximation used in the calculation of this expression is sufficient.

It is clear from eqn. (43) and from the discussion following eqn. (36) that the attenuation of acoustic energy is mainly due to scattering into shear waves. This effect can be calculated in a way similar to the above calculations. For outgoing shear waves the absolute value of the wave-vector $k' = 2\pi f/C_s$ is much larger than the one for the incoming acoustic wave,

$$k' >> k. \tag{44}$$

Therefore:

$$\boldsymbol{q} \approx -\boldsymbol{k}'. \tag{45}$$

This simplifies the calculations significantly, leading to the following expression for the fraction of acoustic energy scattered into shear waves:

$$di_s = d\ell\, \frac{1}{2}(4\pi)^4 \frac{r_{gr}\, r_c^2}{C_s C_\ell^3}\left(\frac{C_{gr}}{C_s}\right)^4 \left(\frac{r_{gr}}{r_c}\right)^\eta \frac{f^4\, (\sin\theta\cos\theta)^2\, d\cos\theta}{1 + (2\pi r_c/C_s)^2\, f^2} \quad . \tag{46}$$

Integrating this expression over all angles results in

$$di_s = d\ell\, \frac{16}{15} 32\, \pi^4 \frac{r_{gr}\, r_c^2}{C_s\, C_\ell^3}\left(\frac{C_{gr}}{C_s}\right)^4 \left(\frac{r_{gr}}{r_c}\right)^\eta \frac{f^4}{1 + (2\,\pi\, r_c/C_s)^2\, f^2} \quad . \tag{47}$$

In order to relate this expression to the attenuation, the definition of *di* should be recollected, eqn. (33),

$$dJ = J\, di \; . \tag{48}$$

Integrating this, results in

$$J = J_o\, exp\, (-\int di) \; , \tag{49}$$

or

$$-\ell n\, (J/J_o) = \int di \; . \tag{50}$$

These results are compared to experimentally derived data in Section 4.

Phase variations

For the purpose of order of magnitude evalutation, phase variations are studied according to the eikonal approximation (Aki and Richards, 1980; Landau and Lifshitz, 1980b). The eikonal approximation yields accurate results if media properties vary smoothly

$$\partial C^2 << C^2 / \lambda , \tag{51}$$

where λ is the wavelength. This inequality is equivalent to

$$\frac{\delta C^2}{C^2} \quad \frac{\lambda}{r_c} << 1 , \tag{52}$$

where δC^2 is the variation over the correlation length r_c . It can be calculated from eqns. (12) and (13):

$$\delta C^2 = \left[C_{gr}^2 \left(\frac{r_{gr}}{r_c} \right)^{1+\eta} e^{-1} \right]^{1/2} . \tag{53}$$

Combining eqns. (52) and (53) results in the following condition for the validity of the eikonal approximation:

$$\left(\frac{r_{gr}}{r_c} \right)^{(1+\eta)/2} e^{-1/2} \frac{\lambda}{r_c} << 1 . \tag{54}$$

The phase variation $\delta\phi$ in the eikonal approximation relates to travel time variation δT, $\delta\phi = \omega\delta T$. The travel time, T, in the eikonal approximation is simply an integral of the inverse velocity over the raypath:

$$T = \int \frac{d\ell}{C(\ell)} . \tag{55}$$

Here the acoustic velocity $C(\ell)$ varies along the raypath due to rigidity variations

$$\begin{aligned} C(\ell) &= \sqrt{\left(K + \frac{4}{3}\mu + \frac{4}{3}\delta\mu(\ell)\right)\varrho} \\ &= \sqrt{\left(K + \frac{4}{3}\mu\right)/\varrho} + \frac{2}{3} \quad \frac{\delta\mu(\ell)}{\varrho} \sqrt{\frac{\varrho}{K + \frac{4}{3}\mu}} \\ &= C_\ell + \frac{2}{3}\delta\mu(\ell)/\varrho \; C_\ell . \end{aligned} \tag{56}$$

The travel time variation, therefore, is

$$\delta T = -\frac{2}{3} \int d\ell \frac{\delta\mu(\ell)}{\varrho_\ell^3} . \tag{57}$$

This quantity averages to zero. The variance of travel times

$$\sigma_t^2 = \langle (\delta T)^2 \rangle \simeq \frac{4}{9} \int d\ell_1 \, d\ell_2 \, \frac{\langle \delta\mu(\ell_1) \, \delta\mu(\ell_2) \rangle}{\varrho^2 C^6} \tag{58}$$

can be calculated using the correlation function in eqns. (12) and (13):

$$\sigma_t^2 \simeq \frac{4}{9} \frac{C_{gr}^4}{C_\ell^6} \int_{r_{gr}}^{\ell} dx\, G(x) \int_0^{\ell} d\ell \simeq \frac{4}{9} \frac{C_{gr}^4}{C_\ell^6} \ell\, r_{gr}\, \ell n \frac{\ell}{r_{gr}} . \qquad (59)$$

The expression on the right here is an approximation suitable for $\ell << r_c$, which is applicable to the transitional layer in the ice. The comparison of eqn. (59) with experimentally derived data is performed in Section 4 using numerical integration.

COMPARISON OF THE MODEL PREDICTIONS TO EXPERIMENTALLY DERIVED DATA

In this section the predictions of our model will be compared with experimentally derived data. These data were derived or compiled in the past by other researchers (Urik, 1983; Duckworth and Baggeroer, 1986) relying on ray theory.

It should be noted that the quantitative predictions of the developed model depend on values of the parameters used below. Some of these values are not known exactly for particular conditions of the experiments so average regional values are used in our calculations. The developed model should, therefore, be expected to provide phenomenological descriptions and interrelations between various quantities, and order-of-magnitude estimation of the discussed effects. The fact that the quantities calculated below came very close to the values estimated from the experimental data should not be taken too seriously at present because of the uncertainties in parameter values. Other effects, such as scattering by ice keels, are expected to be important as well. Notwithstanding these comments, the good correspondence between our theoretical results and the experimentally derived data gives an additional support to our theory.

First, we summarize and discuss the values of the model parameters used for data comparison. For the under-ice transient layer:

$$\begin{aligned} &r_{gr} \approx 2\ cm \\ &C_{gr} = 1.8\ km/s \\ &C_\ell = 1.5\ km/s \\ &r_c \approx 20\ m \\ &C_s \approx 0.46\ km/s \\ &h \approx 0.4\ m \\ &\ell \approx 0.8\ m \end{aligned} \qquad (60)$$

Here $\approx$ indicates approximately known parameters; the ice grain size r_{gr} is taken as estimated in eqn. (9); the shear wave grain velocity C_{gr} is taken as an average value with respect to ice crystal orientation; the acoustic velocity in a transitional layer, C_ℓ, is taken to be equal to the acoustic velocity in water because the rigidity of a transitional layer is small and its compressibility is mostly due to water; the correlation length r_c was estimated for the Arctic in Mellen and Di Napoli (1984); the shear wave velocity in the transitional layer C_s is calculated in eqn. (20); the thickness of the transitional layer h is estimated between 0.2m (Stein, 1988, private communication) and 0.6m (Floyd, 1988, private communication), and the raypath ℓ in the transitional layer per one bounce of a wave is taken as double its thickness because of the near vertical direction of wave propagation due to the upward refraction.

For the unconsolidated sedimentary layer at the bottom:

$$\begin{aligned} r_{gr} &\approx 0.05\ mm \\ C_{gr} &= 2.0\ km/s \\ C_{\ell} &= 1.53\ km/s \\ C_{s} &\approx 0.2\ km/s \\ r_{c} &\approx 1.5m \\ h &\approx 35m \\ \ell &\approx 140\ m. \end{aligned} \tag{61}$$

Here, all parameters but ℓ are taken as regional averages characteristic of the silty sediments of the Arctic Abyssal Plane (Hamilton, 1980; Vogt, 1986); the raypath ℓ in the bottom depends on propagation details such as velocity profile and number of multiple reflections, it is estimated for particular experimental conditions of Duckworth and Baggeroer (1986) per one bounce off the bottom for the 9-th multiple raypath using the raypath calculations in that paper.

Substituting these values into eqn. (47) results in the following. The value of the average fraction of scattered acoustic energy under ice per one bounce of acoustic wave off the ice cover is

$$i^{ice} = 0.64 \cdot 10^{-4} f^2, \text{ for } f \geqslant 10 \text{ Hz}. \tag{62}$$

Sea bottom attenuation for the experimental conditions of Duckworth and Baggeroer (1986) is

$$i^{bottom} = 3.4 \cdot 10^{-4} f^2, \text{ for } f \geq 10 \text{ Hz}. \tag{63}$$

At frequencies lower than 10 Hz, a more complicated frequency dependence is predicted $\sim f^4 / (1 + af^2)$, however, no experimental data have been available to verify this prediction.

We first compare the predicted attenuation due to the under-ice transitional layer to the Arctic transmission loss data published by Urick (1983). According to the Arctic propagation data survey in this book (Fig. 6.19, p. 171) most of acoustic energy in the Arctic travels in a ray bundle which bounces off the ice surface once per 6000 m on average. Therefore, the transmission loss at range R can be written as:

$$\begin{aligned} 10 \log J_R / J_o = &(\text{geometric spreading loss}) \\ &+ (\text{ice attenuation loss}), \end{aligned} \tag{64}$$

where the last item is given by

$$(\text{ice attenuation loss}) = 10 \log \left[\exp \left(-\frac{R}{6000} i^{ice} \right) \right] . \tag{65}$$

This ice attenuation loss can be compared to the total transmisison loss data (Urick, 1983; fig. 6.20, p. 172), by assuming that the geometrical spread is of a cylindrical nature R^{-1} for the range $R > R_o$. The value of R_o can be estimated for the Arctic environment using a model described in Urick (1983, p. 153),

$$R_0 \approx 1.2 \text{ km}. \tag{66}$$

Results of these calculations are summarized in the Table for the frequency 20 Hz (which dominates long range propagation) and for range values of 100 and 1000 km.

Table - Comparison of model and experimental data (F = 20 Hz)

Range	100 km	1000 km
Model Transmission Loss	−1.8 db	−18 db
Experimental Transmission Loss	−1.0 ± 5 db	−11 ± 5 db

These results demonstrate a good correspondence between the model predictions and the measured transmission loss.

Second, we compare predictions of our model to the experimentally derived data on attenuation and travel-time (phase) variations due to interaction with rough under-ice and bottom surfaces in a long range propagation experiment in the Arctic Ocean. A slushy transitional layer was detected under ice in this experiment.

A single explosive shot was used in this experiment, and the analysis of signals arriving via several multiple reflection paths allowed the isolation of the attenuation per single bounce due to scattering effects under-ice and in the bottom. The ice and bottom effects were not separated; the combined effect estimated using the constrained inversion procedure resulted in

$$(i^{ice} + i^{bottom}) \text{ estimated} \approx 3 \cdot 10^{-4} f^2. \tag{67}$$

Again this value is in a good correspondence with the combined effect of our model predictions, eqns. (62) and (63).

Another effect estimated is the random travel-time variation, σ_t, due to the interaction with rough boundaries. The attempt to estimate this parameter using the unconstrained inversion procedure was not successful and it led Duckworth and Baggeroer (1986) to believe that the models used for the inversion (Fresnel and Fraunhofer) did not provide the correct parameterization. The standard deviation of travel-time variations was estimated in Duckworth and Baggeroer (1986) by fitting the estimated spectral null depths to the measured values. Neglecting scattering losses resulted in the estimated value of $\sigma_t = 1$ ms, while assuming a large scattering loss of 35% resulted in $\sigma_t = 0$. Therefore, a physically meaningful estimation is

$$\sigma_t \lesssim 1 ms. \tag{68}$$

This is now compared to the predictions of our model derived previously. First, we verify the region of applicability of eikonal approximation used in this section. Substituting values of eqns. (60) and (61) in eqn. (54) results in the following constraints:

$$\begin{gathered} \text{under ice } f > 10 \text{ Hz}, \\ \text{sea bottom } f > 30 \text{ Hz}. \end{gathered} \tag{69}$$

Since the spectral nulls used to estimate travel-time are located at frequencies near and

above 30 Hz, the eikonal approximation is sufficient for an approximate comparison. Using eqn. (59) results in the following model predictions:

$$\begin{aligned} &\textit{under ice } \sigma_t \approx 0.34 \textit{ ms} \\ &\textit{sea bottom } \sigma_t \approx 0.22 \textit{ ms}. \end{aligned} \tag{70}$$

The combined effect of under-ice and sea-bottom surfaces again is in good agreement with the value estimated from the data in eqn. (68).

In conclusion, our theory is in good agreement with the available data on Arctic transmission loss and phase variation. Analysis using Fraunhofer or Fresnel theories have indicated that an explanation of scattering effects requires an order of magnitude larger r.m.s. roughness than the explanation of random travel-time effects in the same data. Our theory is unique in the reconciliation of this problem by explaining relatively large scattering effects due to acoustic energy conversion into shear waves, and relatively small travel-time effects due to relatively weak effects of rigidity variations on the velocity of acoustic waves. These qualitative considerations give strong support to our theory.

CONCLUSION

Scattering of underwater acoustic waves by the sea bottom and ice cover has been considered in the past by a number of authors; some of these prior publications have been referenced throughout the paper. A novel aspect of the theory developed in this publication is that the rough boundaries are not considered as rigid surfaces, but are characterized by the volumetric distributions of rigidity variations in the transitional layers. These variations are shown to be determined by the second order phase transitions between rigid and nonrigid phases. These variations lead to strong scattering of acoustic waves.

In a recent paper, Di Napoli and Mellen (1986) compared transmission loss calculations using various models with experimental results for low-frequency propagation under a rough ice cover in an Arctic environment; they concluded that the available theories could not account for relatively high observed losses. Their conclusion underscores the importance of results obtained in the current research: good agreement with the experimental data has been obtained using our novel theory of rigidity variations in transitional layers, theoretically explaining a high transmission loss in the Arctic.

A theory of rigidity variations in an unconsolidated sedimentary layer was first developed by the author in the preceding publication (Perlovsky, 1986). It explained certain phenomena observed in geophysical seismology, which had not been explained before. A theory of rigidity variations in a transitional underice layer developed here accounts for a turbulent energy present in arctic under-ice environment. It leads to calculation of an ice grain size in agreement with experimental data, which was not previously explained. This part of the theory can also be related to the generation of frazil ice. The generation of frazil ice, however, occurs at different conditions than those considered in this paper for the relatively thin transitional layer at the bottom of the ice cover.

Future experimental work should study the distribution, abundancy, and acoustic properties of transitional layers, including a comparison to the predicted angular distributions of the scattered field. Future theoretical work should take into account all propagating modes, and develop, if necessary, field theoretical methods, which surpass the limitations of ray theory and finite order perturbation methods. Also the Arctic ambient noise models and optimized signal processing techniques should be developed accounting for the properties of transitional layers.

Acknowledgements. This work was supported by the Naval Sea Systems Command. I appreciate the support and permission to publish the paper. L.P. Tsang helped with numerical calculations. Discussions with A.B. Baggeroer, B. Burdick, G.L. Duckworth, E.R. Floyd, P.W. Smith Jr., P.J. Stein, and M. Wengrovitz were helpful, and I am glad to express my appreciation.

REFERENCES

Aki K. and Richards P.G.; 1980: *Quantitative seismology.* W.H. Freeman and Co., San Francisco.

Broadbent S.R. and Hammersley H.R.; 1976: *Percolation processes.* Proc. Camb. Phil. Soc., **53**, 629-641.

Cherepanov N.V.; 1957: *Determination of the age of drifting ice by optical study of the crystals.* Problemy Arktiki, **2**, 179-184.

Colot J.L., Loodts J.A.C. and Brout R.; 1975: *Critical indices in three dimensions.* J. Phys. A, **8**, 594-608.

Diachok O.I.; 1976: *Effects of Sea-Ice Ridges on sound propagation in the Arctic Ocean.* J. Acoust. Soc. Am., **59**, 1110-1120.

Di Napoli F. and Mellen R.H.; 1986: *Low frequency attenuation in the Arctic Ocean.* In: Akal T. and Berkson J. (eds), Ocean Seismo-Acoustics, Plenum, New York.

Duckworth G.L. and Baggeroer A.B.; 1986: *Estimation of ice surface scattering and acoustic attenuation in Arctic sediments from long-range propagation data.* Ocean Seismo-Acoustics, Akal and Berkson (eds.), Plenum Press, NY.

Einstein A.; 1910: *Theorie der Opaleszenz von homogenen Flussigkeiten and Flussigkeitgemischen in der Nahe des kritischen Zustandes.* Ann. d. Phys., **27**, 1275-1298.

Greene R.R.; 1984: *Ice statistics and acoustic scattering in the Arctic Basin.* SAIC Report, McLean, Virginia.

Gow A.J., Tuker W.B. III and Weeks W.F.; 1987: *Physical properties of summer Sea Ice in the Fram Strait.* June-July 1985. CRREL Report 87-16.

Hamilton E.L.; 1976: *Shear wave velocity versus depth in marine sediments: a Review.* Geophysics, **41** 985-996.

Hamilton E.L.; 1980: *Geoacoustic modeling of the sea floor.* J. Acoust. Soc. Am., **68**, 1313-1340.

Hibler W.D. III and LeSchack L.A.; 1972: *Power spectrum analysis of undersera and surface Sea-Ice profiles.*J. of Glaciology **11**, 345-356.

Hibler W.D. III, Weeks W.F. and Moch S.J.; 1972: *Statistical aspects of Sea-Ice Ridge distributions.* J. Geophysical Res., **77**, 5954-5970.

Hobbs R.V.; 1974: *Ice physics.* Clarendon Press. Oxford.

Hunkins K.; 1980: *Review of the AIDJEX Oceanographic Program.* In: Sea Ice Processes and Models, R.S. Pritchard (ed.), 34-45, Univ. of Washington Press, Seattle.

Kasteleyn P.W. and Fortuin C.M.; 1969: *Phase transitions in lattice systems with random local properties.* J. Phys. Soc. Japan, **26**, 11-14.

Koch R.A., Vidmar P.J. and Lindberg J.B.; 1983: *Normal mode identification for impedance boundary conditions.* J. Acoust. Soc. Am., **73**, 1567-1570.

Kuperman W.S. and Schmidt H.; 1986: *Rough surface elastic wave scattering in a horizontally stratified ocean.*J. Acoust. Soc. Am., **79**, 1767-1777,

Lambe T.W. and Whitman R.V.; 1969: *Soil mechanics.* John Wiley & Sons., New York.

Landau L.D. and Lifshitz E.M.; 1980a: *Statistical physics.* Pergamon Press, London.

Landau L.D. and Lifshitz E.M.; 1980b: *The classical theory of fields.* Pergamon Press, London.

Landau L.D. and Lifshitz; 1980c: *Theory of elasticity.* Pergamon Press, London.

Levinshtein M.E., Shklovsky B.I., Shur M.S. and Efros A.L.; 1975: *The relation between the critical exponents of percolation theory.* Sov. Phys. JETP, **42**, 197-200.

Mellen R.H.; 1966: *Underwater acoustic scattering from Arctic Ice.* J. Acoust. Soc. Am., **40**, 1200-1202.

Mellen R.H. and Di Napoli F.R.; 1984: *Underwater acoustics in the Arctic ocean.* NATO Advanced Study Institute, in Adaptive Methods in Underwater Acoustics.

Morse P.M. and Feshbach H.; 1953: *Methods of theoretical physics.* McGraw-Hill Book Co., New York.

Ornstein L.S. and Zernicke F.; 1916: In: *Electrodynamics of continuous media.* 1980. Landau L.D. and Lifshitz E.M., Addison-Wesley Pressi Reading, Mass.

Perlovsky L.I.; 1986: *Scattering of seismic waves by shear modulus fluctuations due to rigid-nonrigid phase transition.* Boll. Geof. Teor. Appl., **28**, 3-13.

Perlovsky L.I.; 1988: *Field theoretical model for the acoustic propagation with rough bondaries.* NOSC Contract N66001-88-C-0150 Report.

Rothrock D.A. and Thorndike A.S.; 1980: *Geometric properties of the underside of Sea Ice.* J. Geophysical Res., **85**, 3955-3963.

Schmidt H. and Jensen F.B.; 1985: *A Full wave solution for propagation in multi-layered viscoelastic media with application to Gaussian beam reflection at fluid-solid interfaces.* J. Acoust. Soc. Am., **77**, 813-825.

Stanton T.K., Jezek K.C. and Gow A.J.; 1986: *Acoustical reflection and scattering from the underside of laboratory grown Sea Ice: Measurements and Predictions.* J. Acoust. Soc. Am., **80**, 1486-1494.

Urick R.J.; 1983: *Principles of underwater sound.* McGraw-Hill Book Company, New York.

Vogt P.R.; 1986: *Seafloor topography, sediments, and paleoenvironments.* In: Hurdle B.G. (ed), The Nordic Seas, Springer-Verlay, New York.

Wadhams P.; 1981: *Sea-Ice Topography of the Arctic Ocean in the region 70°W to 25° E.* Philosophical Transactions of the Royal Society of London, **302**, 45-85.

Weast R.C.; 1981: *CRC Handbook of chemistry and physics.* CRC Press, Boca Raton, Fla.

Weeks W.F.; 1986: *The Physical properties of the Sea Ice Cover*. In: Hurdle B.G. (ed), The Nordic Seas, Springer-Verlag, New York, pp. 88-100.

Weeks W.F. and Mellor M.; 1983: *Mechanical properties of ice in the Arctic Seas*. USACRREL Report.

Wilson K.G.; 1983: *The renormalization group and critical phenomena*. Rev. Modern Physics, **55**, 583-600.